 CMES, vol.93, no.1, pp.1-16, 2013

Theoretical Analysis of a Functionally Graded Shape Memory Alloy Beam under Pure Bending

Lijun Xue[1], **Guansuo Dui**[1,2], **Bingfei Liu**[3]

Abstract: The Functionally Graded Shape Memory Alloy (FG-SMA) is a new kind of functional materials which possesses the excellent properties of both Shape Memory Alloy (SMA) and Functionally Graded Material (FGM). A macro constitutive model of FG-SMA is established by using the theory of the mechanics of composites and the existing SMA model. With this macro constitutive model, the mechanical behavior of a FG-SMA beam composed by elastic material A and SMA subjected to pure bending is investigated. The loading processes including elastic process and phase transformation process are discussed in detail and the analytical solutions are obtained. What is more, a new layered method for establishing the finite element model of the FG-SMA beam is provided. The theoretical results show a good agreement with the experiment data, which indicates that the macro constitutive model and the finite element method provided here are valid. At last, the stress distribution on the cross section, the position of the neutral axis and the curvature-bending moment relation are discussed through numerical results, respectively. The obtained results demonstrate several interesting features of this new material, which may have potential applications in the future. This research can provide a base for the design and in-depth investigation of FG-SMA material.

Keywords: Functionally graded material, Shape memory alloy, Pure bending, Stress distribution.

1 Introduction

Functionally Graded Material (FGM) is a kind of inhomogeneous composites which is usually made from two or more constituent phases with a continuously variable composition. FGM holds a number of excellent features that make them attractive

[1] Institute of Mechanics, Beijing Jiaotong University, Beijing 100044, China.
[2] Corresponding author.
Tel.: +1-86-1051688437; fax: +1-86-1051682094. E-mail: Gsdui@center.njtu.edu.cn
[3] Airport College, Civil Aviation University of China, Tianjin 300300, China.

in potential applications, such as the stress singularities elimination, higher fracture toughness, and enhanced thermal properties. A number of papers considering various aspects of FGM have been published in recent years [Sanaka (2001); Tarn (2001); Ding, Huang and Chen (2007)]. Shape Memory Alloy (SMA) is a kind of intellectual materials developed in recent years. Due to its particular shape memory effect and pseudo-elasticity, SMA has been widely used in biomedical science, aerospace, robotics and other areas. All these particular characteristics go together with the formation of martensitic microstructures. SMA possesses the ability to transform spontaneously between the austenitic and martensitic variants under a variety of temperature or stress. In order to understand the transformation principle and make good use of the superior properties, many researches ranging over various aspects of SMA have been carried out in the past several years [Tanaka (1986); Liang and Rogers (1990); Brinson (1993); Sun and Hwang (1993); Boyd and Lagoudas (1994); Liu, Dui and Zhu (2011); Chen, Peng, Chen, Wang, Wang and Hu (2012)].

The Functionally Graded Shape Memory Alloy (FG-SMA) is a new kind of composites which possesses the excellent properties of both SMA and FGM. Such as a kind of FG-SMA medical guide wire, the tip portion of the guide wire must be sufficiently flexible to pass through the meandering blood vessels, so that the medical instruments can be introduced into a desired site: soft vessels in the brain, heart, liver, etc. On the other hand, from the middle to the end of the guide wire, high strength against bending is also required to overcome the high resistance to bending and rotation in a blood vessel and to smoothly transmit the torque from the end to the tip of the guide wire [Sutou, Omori and Furukawa (2004)]. FG-SMA can be divided into two categories according to the constituents and the structure of the material: One is mixing SMA with other materials and the volume fraction of SMA changing gradually, thus producing the FG-SMA [Burkes and Moore (2007); Cole, Bruck and Roytburd (2008); Tian and Schryvers, (2009)]; The other is produced by processing the SMA with special technics to change the inner microstructure of SMA, so as to create the FG-SMA with gradually varying properties [Mahmud, Liu and Nam (2008); Birnbaum, Satoh and Yao (2009)].

A thorough understanding of the mechanical behavior of FG-SMA is needed for the rapid increasing requirement in high and new technology applications, and several articles which study the properties of this new material have been published recently. Birnbaum, Satoh and Yao (2009) introduced a new process and mechanism which can control the shape memory response spatially within monolithic NiTi thin film structures. This technique is shown to effectively control the martensitic phase transformation temperature and exhibits control over aspects of the mechanical and shape memory responses as well. Mahmud, Liu and Nam (2008) reported a novel

heat treatment method for the creation of functionally graded near-equiatomic NiTi SMA. This method is an anneal within a temperature gradient after cold work, thus creating a structural gradient within the matrix of the SMA. Tian and Schryvers (2009) developed a new "hot" target approach to fabricate functionally layered or graded material. Cole, Bruck and Roytburd (2008) gave out a method by depositing $Ni_{47}Ti_{53}$ films of varying thickness onto $Ni_{56}Ti_{44}$ substrates and annealing the films to produce compositional gradients through diffusion modification. And nanoindentation measurements were used to probe the mechanical properties at various depths into the film. However, the existing researches all concentrate on the fabrication and performance test of the FG-SMA, there is still not a reasonable constitutive model or method to describe the mechanical properties of this kind of material. So, in depth study is still necessary to reveal and predict the mechanical behavior of FG-SMA.

In this paper, a macro constitutive model which can describe the mechanical characteristic of FG-SMA is provided, and using this constitutive model, the mechanical behavior of the FG-SMA beam which is composed by elastic material A and SMA subjected to pure bending is investigated. With the purpose of getting the analytical solutions, a power-law function is proposed to describe the volume fraction of SMA. Furthermore, according to the theory of the mechanics of composites, the average stress is obtained by considering the stress of each component of the material, and the stress-strain relationship of SMA is described by an ideal phase transformation model. With the balance equations of the stress and bending moment and the boundary conditions, the neutral axis y_0, the curvature k and the critical layer h_1 and h_2 can be got and then the stress distribution on the cross section can be derived. In the end, the influence of the distribution function and the bending moment on the stress distribution and the neutral axis is discussed through numerical results, respectively. It can be studied that the stress field at the phase transformation area of FG-SMA is quite different from the common FGM beam, and the maximum stress decreases notably. It can be concluded that the destruction caused by oversize stress may be prevented efficiently by displaying SMA at a suitable position of the structural component. This paper can not only display the mechanical behavior of the FG-SMA beam but also provide a base for the in-depth study of this kind of material.

2 Theoretical analysis

The model is considered as a FG-SMA rectangular cross section beam which is subjected to a pure bending M. The width and height of the cross section are b and h, respectively, and the length from the neutral axis to the bottom of the cross section is y_0, as shown in Fig. 1. The FG-SMA beam consists of elastic material A

and SMA, and the distribution function of the SMA is $f(y)=(y/h)^n$ ($n>0$). With the increasing of M, the beam will undergo a process from elastic deformation to phase transformation. In order to study the performance of the FG-SMA beam during the whole process, it is assumed that the cross section of the beam keeps flat through the whole bending process.

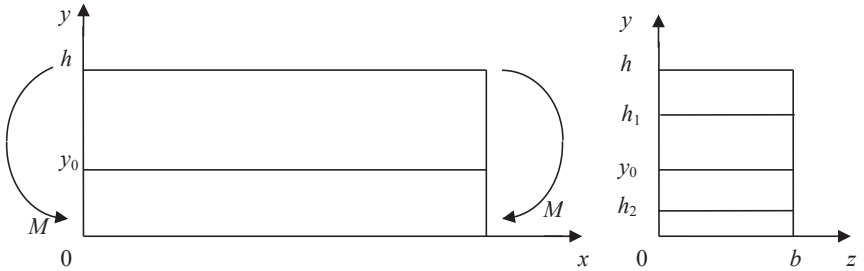

Figure 1: The FG-SMA beam subjected to pure bending

2.1 Elastic analysis

According to the assumption of plane cross-section, the strain of the cross section is

$$\varepsilon = k(y - y_0) \tag{1}$$

where k is the curvature.

Under a small bending moment M, the material is in elastic stage. The stress of material A is obtained by

$$\sigma_0 = E_0 \varepsilon \tag{2}$$

and the stress of SMA is obtained by

$$\sigma_1 = E_A \varepsilon \tag{3}$$

where E_0 and E_A are the elastic moduli of the material A and the austenite of SMA, respectively.

Several micromechanical models for heterogeneous materials have been developed recently [Dong and Atluri (2011); (2012)]. However, when these models are used for FG-SMA, the integral equations are too complicated to be solved. In order

to simplify the calculation, the average stress of the FG-SMA beam is expressed according to the theory of mechanics of composites as

$$\sigma = [1 - f(y)]\sigma_0 + f(y)\sigma_1 \tag{4}$$

The balance equation of the stress $\int_0^h \sigma b \mathrm{d}y = 0$ is:

$$\int_0^h [E_0 + f(y)(E_\mathrm{A} - E_0)]k(y - y_0)b\mathrm{d}y = 0 \tag{5}$$

The balance equation of the bending moment $\int_0^h \sigma y b \mathrm{d}y = M$ is:

$$\int_0^h [E_0 + f(y)(E_\mathrm{A} - E_0)]k(y - y_0)yb\mathrm{d}y = M \tag{6}$$

Through these two equations (5) and (6), the neutral axis y_0 and the curvature k are obtained:

$$y_0 = \frac{(n+1)(nE_0 + 2E_\mathrm{A})}{2(n+2)(nE_0 + E_\mathrm{A})}h \tag{7}$$

$$k = \frac{12(n+3)(n+2)^2(nE_0 + E_\mathrm{A})}{12E_\mathrm{A}^2 + n^2(n^2+4n+7)E_0^2 + 4n(n^2+4n+7)E_0E_\mathrm{A}} \cdot \frac{M}{bh^3} \tag{8}$$

Then the stress distribution on the cross section is obtained:

$$\sigma = k[\frac{E_\mathrm{A} - E_0}{h^n}y^{n+1} - \frac{E_\mathrm{A} - E_0}{h^n}y_0y^n + E_0y - y_0E_0] \tag{9}$$

According to (7), it can be calculated that for the case of n=0, the neutral axis $y_0 = h/2$ and the beam is homogeneous and composed only by SMA. While for the case of $n \to \infty$, the same value of the neutral axis can be got, and the beam is composed only by material A.

2.2 Phase transformation analysis

With the increasing of M, the stress of SMA (σ_1) will reach the start stress of martensitic transformation σ_s, and the corresponding bending moment can be figured out. Since SMA is asymmetric of tension and compression, the critical stresses of the start and finish of martensitic transformation are different. Here we denote the start and finish stresses of martensitic transformation in tension area by σ_st and σ_ft (σ_st, $\sigma_\mathrm{ft} > 0$), and the start and finish stresses of martensitic transformation in compression region by σ_sc and σ_fc (σ_sc, $\sigma_\mathrm{fc} > 0$), respectively.

If the stress σ_1 at the top of the cross section first reaches the start stress of martensitic transformation σ_st and the σ_1 at the bottom of the cross section is less than

σ_{sc}, the condition of this case and the elastic limit bending moment M_s can be got by $|\sigma_1(0)| < \sigma_{sc}$ and $\sigma_1(h) = \sigma_{st}$:

$$\frac{(n+1)(nE_0+2E_A)}{n(n+3)E_0+2E_A} < \frac{\sigma_{sc}}{\sigma_{st}} \tag{10}$$

$$M_s = \frac{\sigma_{st}bh^3}{E_A(h-y_0)} \cdot \frac{12E_A^2+n^2(n^2+4n+7)E_0^2+4n(n^2+4n+7)E_0E_A}{12(n+3)(n+2)^2(nE_0+E_A)} \tag{11}$$

If the stress σ_1 at the bottom of the cross section first reaches the start stress of martensitic transformation σ_{sc} and the stress σ_1 at the top of the cross section is less than σ_{st}, the condition for this case and the elastic limit bending moment M_s can be got by $\sigma_1(h) < \sigma_{st}$ and $\sigma_1(0) = -\sigma_{sc}$.

$$\frac{(n+1)(nE_0+2E_A)}{n(n+3)E_0+2E_A} > \frac{\sigma_{sc}}{\sigma_{st}} \tag{12}$$

$$M_s = \frac{\sigma_{sc}bh^3}{E_Ay_0} \cdot \frac{12E_A^2+n^2(n^2+4n+7)E_0^2+4n(n^2+4n+7)E_0E_A}{12(n+3)(n+2)^2(nE_0+E_A)} \tag{13}$$

When $M > M_s$, the austenite of SMA will transform into martensite. In the transformation range, the relation between the stress and strain of SMA is displayed in Fig. 2, and the average stress can be expressed as

$$\sigma_1 = \left\{ \begin{array}{l} E_A\varepsilon, (\varepsilon \le \frac{\sigma_s}{E_A}) \\ \sigma_s + \frac{\sigma_f-\sigma_s}{\varepsilon^p+\frac{\sigma_f}{E_M}-\frac{\sigma_s}{E_A}}(\varepsilon - \frac{\sigma_s}{E_A}), (\frac{\sigma_s}{E_A} < \varepsilon \le \varepsilon^p + \frac{\sigma_f}{E_M}) \\ E_M(\varepsilon - \varepsilon^p), (\varepsilon > \varepsilon^p + \frac{\sigma_f}{E_M}) \end{array} \right\} \tag{14}$$

where ε^p is the total phase transformation strain.

Here we assume that the austenite of SMA at the top of the cross section transforms into martensite first while the austenite at the bottom of the cross section does not and the transformation range starts from h_1 ($h_1 > y_0$) to the top, as shown in Fig. 1(b). Now the average stress σ of the beam can be expressed as

$$\sigma = \left\{ \begin{array}{l} [E_0 + f(y)(E_A - E_0)]k(y-y_0), (y \le h_1) \\ f(y)\{\sigma_{st} + \frac{\sigma_{ft}-\sigma_{st}}{\varepsilon^p+\frac{\sigma_{ft}}{E_M}-\frac{\sigma_{st}}{E_A}}[k(y-y_0) - \frac{\sigma_{st}}{E_A}]\} + [1-f(y)]E_0k(y-y_0), (y > h_1) \end{array} \right. \tag{15}$$

Thus, the balance equation of the stress $\int_0^h \sigma b \mathrm{d}y = 0$ is:

$$\frac{(nE_0+2A)h^2}{2(n+2)} + \frac{(nE_0+E_A)\sigma_{st}h}{(n+1)E_Ak} - \frac{(nE_0+A)h}{n+1}h_1 - \frac{E_A-A}{(n+1)(n+2)h^n}h_1^{n+2} = 0 \tag{16}$$

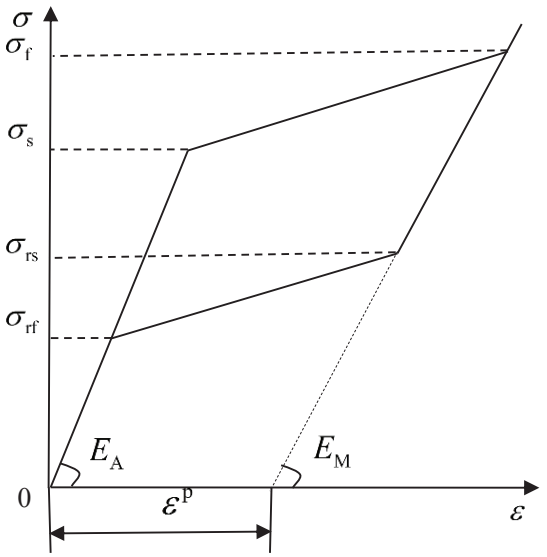

Figure 2: The relation between the stress and strain of SMA

where $A = \frac{\sigma_{ft}-\sigma_{st}}{\varepsilon^p+\frac{\sigma_{ft}}{E_M}-\frac{\sigma_{st}}{E_A}}$.

The balance equation of the bending moment $\int_0^h \sigma y b \mathrm{d}y = M$ is:

$$\frac{(nE_0+3A)h^3}{3(n+3)}+\frac{(nE_0+2E_A)\sigma_{st}h^2}{2(n+2)E_Ak}-\frac{(nE_0+2A)h^2}{2(n+2)}h_1-\frac{E_A-A}{(n+2)(n+3)h^n}h_1^{n+3}=\frac{M}{bk} \tag{17}$$

The stress of the SMA at h_1 reaches σ_{st}: $\sigma_1(h_1)$= σ_{st}

$$E_Ak(h_1-y_0)=\sigma_{st} \tag{18}$$

Through the equations (16), (17) and (18), the k, h_1 and y_0 corresponding to M can be obtained, and then the stress distribution on the whole cross section can be got.

With the increasing of M, the austenite of SMA at the bottom of the cross section will transform into martensite too. Now $\sigma_1(0)$= -σ_{sc}:

$$E_Ak(0-y_0)=-\sigma_{sc} \tag{19}$$

Through the equations (16), (17), (18) and (19), the k, h_1, y_0 and the critical bending moment M can be derived, as well as the stress distribution.

With the keeping increase of M, there are some areas both at the top and the bottom of the cross section in which the austenite transforms into martensite. Now we assume that the transformation range starts from 0 to h_2 ($h_2 < y_0$) and h_1 to h, as shown in Fig. 1(b). Then the average stress σ can be expressed as

$$\sigma = \begin{cases} [1-f(y)]E_0k(y-y_0) - f(y)\{\sigma_{sc} + \frac{\sigma_{fc}-\sigma_{sc}}{\varepsilon^p + \frac{\sigma_{fc}}{E_M} - \frac{\sigma_{sc}}{E_A}}[k(y_0-y) - \frac{\sigma_{sc}}{E_A}]\}, (y \le h_2) \\ [E_0 + f(y)(E_A - E_0)]k(y-y_0), (h_2 < y \le h_1) \\ [1-f(y)]E_0k(y-y_0) + f(y)\{\sigma_{st} + \frac{\sigma_{ft}-\sigma_{st}}{\varepsilon^p + \frac{\sigma_{ft}}{E_M} - \frac{\sigma_{st}}{E_A}}[k(y-y_0) - \frac{\sigma_{st}}{E_A}]\}, (y > h_1) \end{cases} \tag{20}$$

The balance equation of the stress $\int_0^h \sigma b dy = 0$ is:

$$\frac{(nE_0+2A)h^2}{2(n+2)} + \frac{(nE_0+E_A)\sigma_{st}h}{(n+1)E_Ak} - \frac{(nE_0+A)h}{n+1}h_1 - \frac{(E_A-A)h_1^{n+2} - (E_A-B)h_2^{n+2}}{(n+1)(n+2)h^n} = 0 \tag{21}$$

where $B = \frac{\sigma_{fc}-\sigma_{sc}}{\varepsilon^p + \frac{\sigma_{fc}}{E_M} - \frac{\sigma_{sc}}{E_A}}$.

The balance equation of the bending moment $\int_0^h \sigma y b dy = M$ is:

$$\frac{(nE_0+3A)h^3}{3(n+3)} + \frac{(nE_0+2E_A)\sigma_{st}h^2}{2(n+2)E_Ak} - \frac{(nE_0+2A)h^2}{2(n+2)}h_1 - \frac{(E_A-A)h_1^{n+3} - (E_A-B)h_2^{n+3}}{(n+2)(n+3)h^n} = \frac{M}{bk} \tag{22}$$

The stresses of SMA at h_2 and h_1 reach the start stress of martensitic transformation: $\sigma_1(h_2)$= -σ_{sc} and $\sigma_1(h_1)$= σ_{st}

$$E_Ak(h_2 - y_0) = -\sigma_{sc} \tag{23}$$

$$E_Ak(h_1 - y_0) = \sigma_{st} \tag{24}$$

Through the equations (21), (22), (23) and (24), the k, h_1, h_2 and y_0 corresponding to M can be obtained, and then the stress distribution on the whole cross section can be got.

Continuing to increase the bending moment M, the SMA in both top and bottom of the cross section will finish the phase transformation. Thus, the cross section can be divided into five regions: two total transformation regions in the tension and compression area, two partially transformation regions in the tension and compression

area and an elastic region where no austenite of SMA transforms into martensite. The analysis of this condition is similar to the stages studied above and the corresponding curvature, neutral axis and the critical layers between each region can be derived using the same approach, as well as the stress distribution on the cross section.

3 Finite element analysis

Compared to common FGM, the mechanical property of FG-SMA varies not only with the position of the material but also with the temperature and the load. In order to get the accurate results and avoid complex calculation as well, a layered method is used here to establish the finite element model of the FG-SMA beam. First, divide the cross section of the beam into m layers with uniform thickness along the gradient direction, and the volume fraction of SMA of each layer is determined by the distribution function of SMA $f(y)$. Then divide each layer into two sublayers, representing SMA and material A respectively, and the thickness of each sublayer is determined by the volume fraction of SMA of this layer. With the increasing of m, the obtained result will be more and more accurate. The finite element model of this FG-SMA beam as displayed in Fig. 3 is established and calculated with the finite element software ANSYS 14.0.

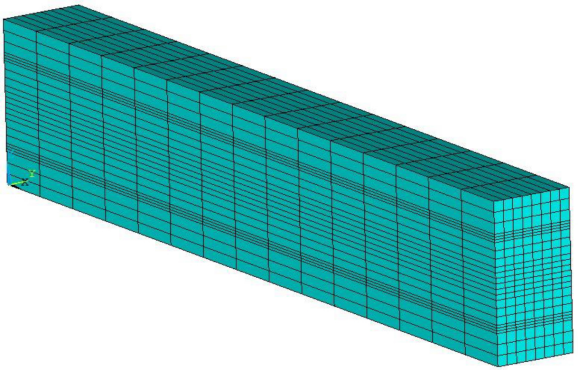

Figure 3: The finite element model of the FG-SMA beam

4 Numerical examples and discussion

In order to check the validity of this macro model, the present model is used to calculate the stress-strain relation of common SMA composite first due to lack of experiment data of FG-SMA, and the obtained theoretical results are compared with

the experiment data [Hamada, Lee, Mizuuchi, Taya and Inoue (1998)], as shown in Fig. 4. It is not difficult to see that the difference between the theoretical results and the experiment data is very little, which shows that the present macro model is valid to predict the mechanical behavior of SMA composite. Since the curve of the theoretical results consists of two straight lines, the present model can be used to predict the mechanical behavior of FG-SMA efficiently for this simplicity, eliminating the calculating iteration of other complex models.

For the purpose of explaining this theory clearly, some numerical examples of the FG-SMA beam are given here. The width and height of the cross section are b=50 mm and h=100 mm. The elastic moduli of the austenite, martensite and material A are E_{A}=70GPa, E_{M}=30GPa and E_0=210GPa [Bo, Lagoudas and Miller (1999)], respectively. The total phase transformation strain ε^{P}=0.069, and the critical stresses are σ_{st}=290Mpa, σ_{ft}=380MPa, σ_{sc}=350MPa and σ_{fc}=600MPa [Zhu and Dui (2010)], respectively.

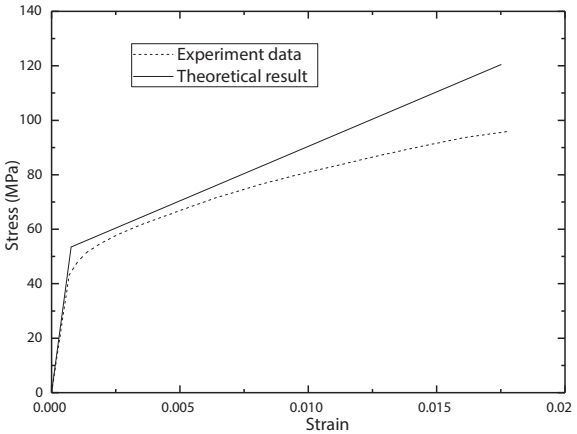

Figure 4: The stress-strain curves of common SMA composite (experiment data and theoretical results)

4.1 The distribution of the stress on the cross section

In order to reveal the property of the stress distribution on the cross section of the FG-SMA beam, three figures are given out here. In Fig. 5, the solid curve represents the stress distribution of the FG-SMA beam considering the phase transformation behavior of SMA while the dash curve represents the stress distribution of the same beam in which the transformation behavior of SMA is ignored. And the dot line represents the stress distribution obtained by the finite element method.

It can be learned from Fig. 5 that the maximum tension stress of the FG-SMA beam is reduced compared to the beam in which the transformation property of SMA is omitted subjected to the same bending moment, while the maximum of the compression stress is increased a little. It can also be seen that the theoretical results have a good agreement with the finite element results, which reveals that the method provided in section 3 to establish the finite element model is valid. It is easy to get the conclusion that the FG-SMA beam can have a small tension stress under pure bending moment. Although the compression stress is increased, it is known to us that there are some materials such as ceramic which have a better anti-pressure ability than tensile capacity, so we can take full advantage of this property in this kind of material.

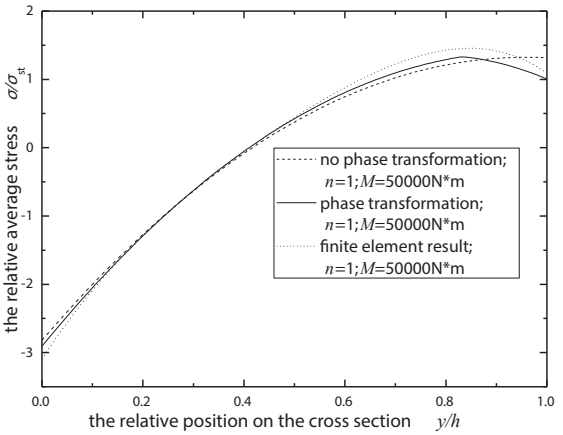

Figure 5: The stress distribution on the cross section of the FG-SMA beam (considering and not considering the phase transformation of SMA)

Fig. 6 reveals the distribution characteristic of the stress on the cross section of the FG-SMA beam with the same n but different M. It can be studied that the capability to reduce the maximum stress of FG-SMA beam increased with the increasing bending moment M, as well as the material advantage of FG-SMA. Fig. 7 displays the distribution characteristic of the stress with the same M but different n. It is easy to find that the stress distribution on the cross section is effected remarkably by the SMA distribution function (different n). The most suitable FG-SMA material can be designed by selecting the reasonable SMA distribution function according to the practical application, making full use of the material.

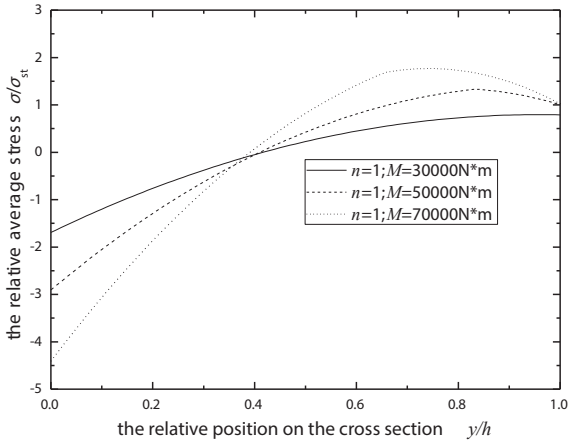

Figure 6: The stress distribution on the cross section of the FG-SMA beam (the same n with different M)

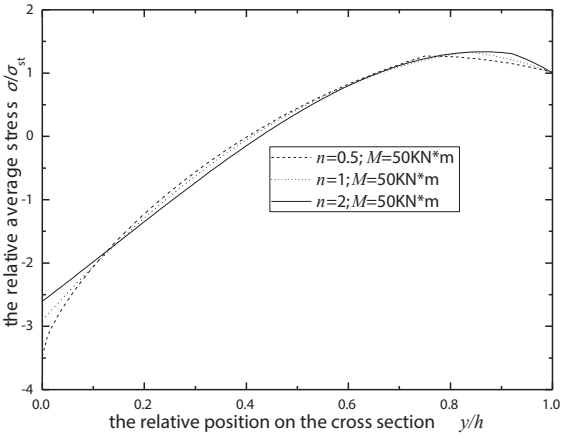

Figure 7: The stress distribution on the cross section of the FG-SMA beam (the same M with different n)

4.2 The position of the neutral axis

With different n and M, the position of the neutral axis of the cross section is different. The regular pattern is displayed in Fig. 8. It can be learned that the position of the neutral axis is unchangeable when $M<M_s$, while it descends when $M>M_s$ and it approaches to a limit position when $M \to \infty$. It can also be found that the descending speed becomes slow with an increasing n, and the descending amplitude

is decreased too. According to this characteristic, the most reasonable FG-SMA structural element can be designed, improving the using efficiency of this kind of material.

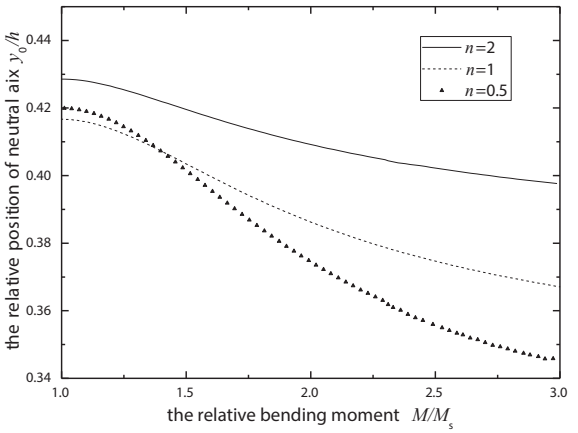

Figure 8: The position of the neutral axis of the FG-SMA beam

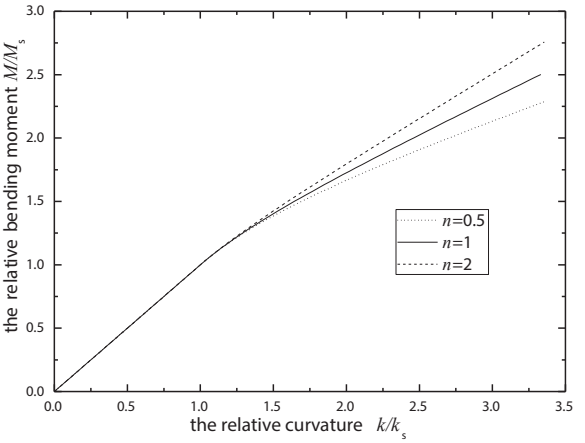

Figure 9: The relation between the curvature and the bending moment

4.3 The relation between M and curvature k

Fig. 9 gives out the variation of the curvature k with the bending moment M. It is easy to conclude that the slope of the curve is one when $M/M_s \leqq 1$, and it approaches

to the slope at which all the austenite in SMA of the beam transformed with the increase of M. What's more, the slope increases with the increase of n.

5 Conclusions

FG-SMA material which possesses the properties of both SMA and FGM is investigated in this paper, and a macro constitutive model which can describe the mechanical behavior of this material is established. With this model, the mechanical behavior of a FG-SMA beam subjected to pure bending is studied in detail. The stress distribution on the cross section and the position of the neutral axis are analyzed through numerical examples, as well as the curvature-bending moment relation. It can be learned that the FG-SMA beam can have a smaller tension stress compared to a common FGM beam due to the transformation of SMA. The position of the neutral axis descends with the increase of bending moment during the transformation process. The stress distribution is effected remarkably by the SMA distribution function. The most rational FG-SMA material can be designed by choosing the appropriate distribution function of SMA to content different demands of actual applications.

Acknowledgement

The authors acknowledge the financial support of National Natural Science Foundation of China (No. 11132003, 11172033, 11272044, 11272136) and National Basic Research Program of China (973 Program) (2010CB7321004), and it is also supported by the scientific research foundation of civil aviation university of China (2013QD08S).

References

Birnbaum, A.J.; Satoh, G.; Yao, Y.L. (2009): Functionally grading the shape memory response in NiTi films: Laser Irradiation. *Journal of Applied Physics*, vol. 106, no. 4, pp. 043504-1-8.

Bo, Z.; Lagoudas, D.C.; Miller, D. (1999): Material characterization of SMA actuators under nonproportional thermomechanical loading. *Journal of Engineering Materials and Technology*, vol. 121, pp. 75-85.

Boyd, J.G.; Lagoudas, D.C. (1994): Thermomechanical response of shape memory composites. *Journal of Intelligent Material Systems and Structures*, vol. 5, pp. 333-346.

Brinson, L.C. (1993): One dimensional constitutive behavior of shape memory alloys: thermomechanical derivation with non-constant material functions. *Journal*

of Intelligent Material Systems and Structures, vol. 4, pp. 229-242.

Burkes, D.E.; Moore, J. (2007): Microstructure and kinetics of a functionally graded NiTi–TiCx composite produced by combustion synthesis. *Journal of Alloys and Compounds*, vol. 430, pp. 274–281.

Chen, B.; Peng, X.; Chen, X.; Wang, J.; Wang, H.; Hu, N. (2012): A three-dimensional model of shape memory alloys under coupled transformation and plastic deformation. *CMC: Computers Materials and Continua*, vol. 30, no. 2, pp. 145-176.

Cole, D.; Bruck, H.; Boytburd, A. (2008): Nanoindentation studies of graded shape memory alloy thin films processed using diffusion modification. *Journal of Applied Physics*, vol. 103, pp. 064315 -1-4.

Ding, H.J.; Huang, D.J.; Chen, W.Q. (2007): Elasticity solutions for plane anisotropic functionally graded beams. *International Journal of Solids and Structures*, vol. 44, pp. 176-196.

Dong, L.; Atluri, S.N.; (2011): Development of T-Trefftz four-node quadrilateral and Voronoi Cell Finite Elements for macro-& micromechanical modeling of solids. *CMES: Computer Modeling in Engineering & Sciences*, vol. 81, no. 1, pp. 69-118.

Dong, L.; Atluri, S.N. (2012): Development of 3D T-Trefftz Voronoi Cell Finite Elements with/without Spherical Voids &/or Elastic/Rigid Inclusions for Micromechanical Modeling of Heterogeneous Materials. *CMC: Computers Materials and Continua*, vol. 29, no. 2, pp. 169-211.

Hamada, K.; Lee, J.H.; Mizuuchi, K.; Taya, M.; Inoue, K. (1998): Thermomechanical behavior of TiNi shape memory alloy fiber reinforced 6061 aluminum matrix composite. *Metallurgical and Materials Transactions A-Physical Metallurgy and Materials Science*, vol. 29, pp. 1127-1135.

Liang, C.; Rogers, C.A. (1990): One-dimensional thermomechanical constitutive relations for shape memory materials. *Journal of Intelligent Material Systems and Structures*, vol. 1, pp. 207-234.

Liu, B.; Dui, G.; Zhu, Y. (2011): A Constitutive Model for Porous Shape Memory Alloys Considering the Effect of Hydrostatic Stress. *CMES: Computer Modeling in Engineering & Sciences*, vol. 78, no. 4, pp. 247-275.

Mahmud, A.S.; Liu, Y.N.; Nam, T. (2008): Gradient anneal of functionally graded NiTi. *Smart Materials & Structures*, vol. 17, pp. 015031(5pp).

Sanaka, B.V. (2001): An elasticity solution for functionally graded beams. *Composites Science and Technology*, vol. 61, pp. 689-696.

Sun, Q.P.; Hwang, K.C. (1993): Micromechanics modeling for the constitutive

behavior of polycrystalline shape memory alloys—I. Derivation of general relations. *Journal of the Mechanics and Physics of Solids*, vol. 41, pp. 1-17.

Sutou, Y.; Omori, T.; Furukawa, A. (2004): Development of Medical Guide Wire of Cu-Al-Mn–Base Superelastic Alloy with Functionally Graded Characteristics. *Journal of Biomedical Materials Research Part B-Applied Biomaterials*, vol. 69, pp. 64-69.

Tanaka, K.A. (1986): Thermomechanical Sketch of Shape Memory Effect: One-Dimensional Tensile Behavior. *Res Mechanica*, vol. 18, pp. 251-263.

Tarn, J.Q. (2001): Exact solutions for functionally graded anisotropic cylinders subjected to thermal and mechanical loads. *International Journal of Solids and Structures*, vol. 38, pp. 8189-8206.

Tian, H.; Schryvers, D. (2009): Fabrication and characterization of functionally graded Ni–Ti multilayer thin films. *Functional Materials Letters*, vol. 2, no. 2, pp. 61-66.

Zhu, Y.P.; Dui, G.S. (2010): A macro-constitutive model of polycrystalline NiTi SMAs including tensile–compressive asymmetry and torsion pseudoelastic behaviors. *International Journal of Engineering Science*, vol. 48, pp. 2099-2106.